Supplementary Material

for

Dendritic fibrous nano-particles (DFNPs): rising stars from mesoporous materials

Yabin Wang,†*[a] Xin Du,†*[b] Zhong Liu,[c] Shihui Shi[a] and Haiming Lv[a]

[a] Shaanxi Key Laboratory of Chemical Reaction Engineering, College of Chemistry and Chemical Engineering, Yan'an University, Yan'an 716000, Shaanxi, P. R. China.

[b] Research Center for Bioengineering and Sensing Technology, School of Chemistry & Biological Engineering, University of Science & Technology Beijing, Beijing 100083, P. R. China.

[c] Key Laboratory of Comprehensive and Highly Efficient Utilization of Salt Lake Resources, Qinghai Institute of Salt Lakes, Chinese Academy of Sciences, Xining 810008, China.

† These authors contributed equally to this work.

* Corresponding authors.

E-mail addresses: ybw_bingerbingo@126.com (Y. B. Wang),
duxin@ustb.edu.cn (X. Du).

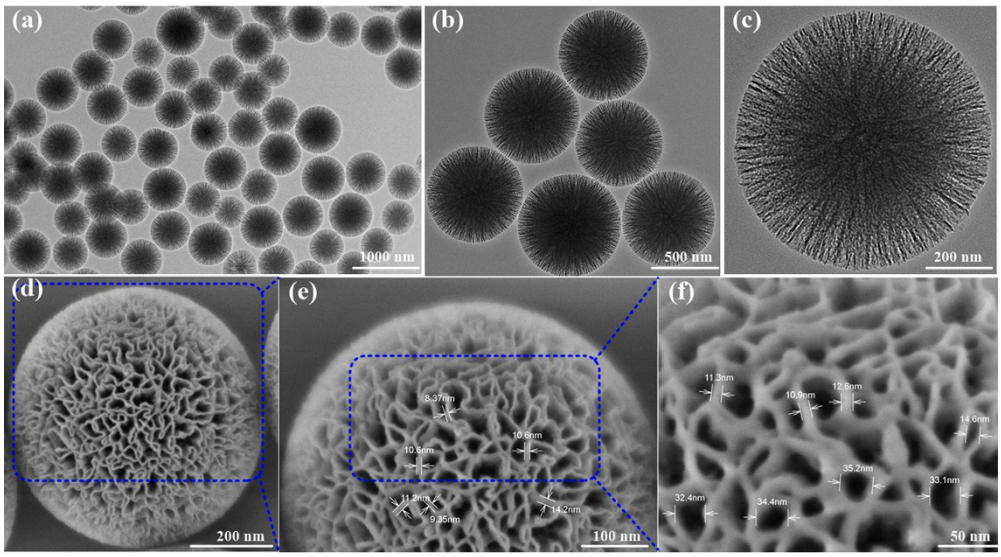

Fig. S1 TEM (a-c) and SEM (d-f) images of silica-based nanospheres with dendritic fibrous morphologies prepared according to a modified cyclohexane emulsion system. The thicknesses of the wrinkled nanosheets and the diameters of the irregular quasi-pores were randomly calibrated, with the former ranging from 8.3 to 14.2 nm (e) and the latter from 10.9 to 35.2 nm (f), respectively. Reproduced from ref. 1 with permission from Harbin Institute of Technology, copyright 2018.

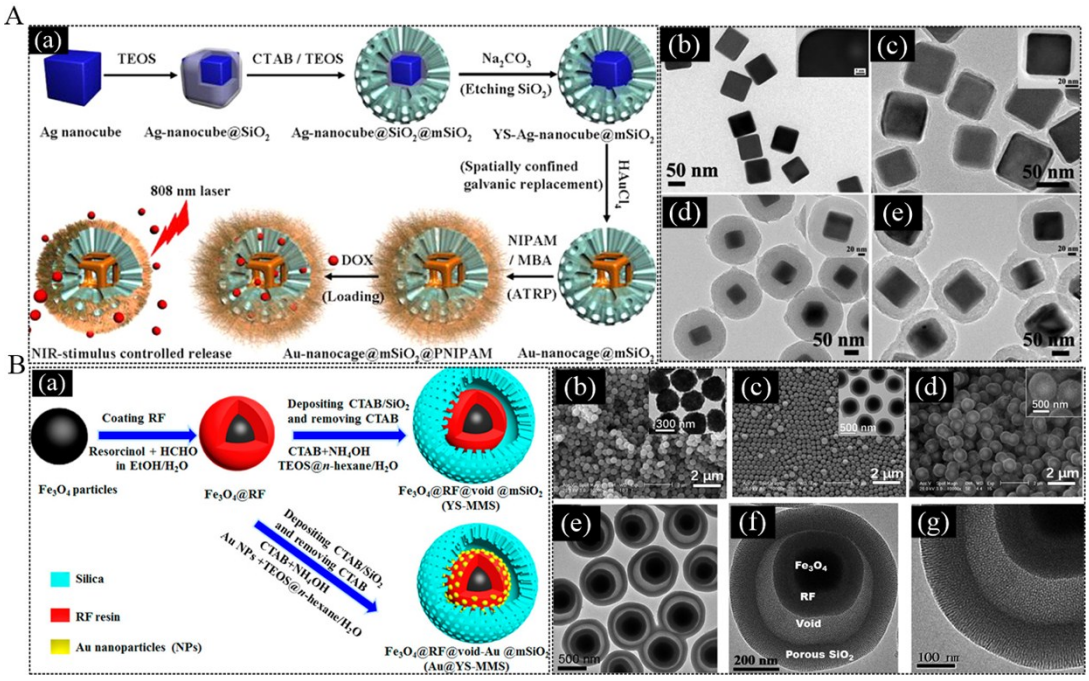

Fig. S2 Core-shelled MSNs with gold nanocages (A) and Fe_3O_4 as cores (B). For A: Schematic illustration of the gold nanocages@mesoporous silica core-shell structure coated with a smart polymer (Au-nanocage@mSiO_2@PNIPAM) for NIR-stimulus controlled drug release (a). TEM images of (b) Ag nanocubes prepared using a NaHS mediated polyol synthesis method, (c) the core-shell Ag-nanocube@SiO_2, (d) Ag-nanocube@SiO_2 @mSiO_2, and (e) YS-Ag-nanocube@mSiO_2 (after etching the middle silica layer to form the yolk-shell (YS) structure). Reproduced from ref. 2 with permission from American Chemical Society, copyright 2017. For B: Synthesis procedure for the YS-MMS microspheres (a). SEM images of Fe_3O_4 (b), Fe_3O_4@RF (c), and YS-MMS (d) microspheres and TEM images (e-g) of YS-MMS-35 with different magnification. The inset in panel (b) and (c) is the corresponding TEM image of Fe_3O_4 and Fe_3O_4@RF microspheres. Reproduced from ref. 3 with permission from American Chemical Society, copyright 2017.

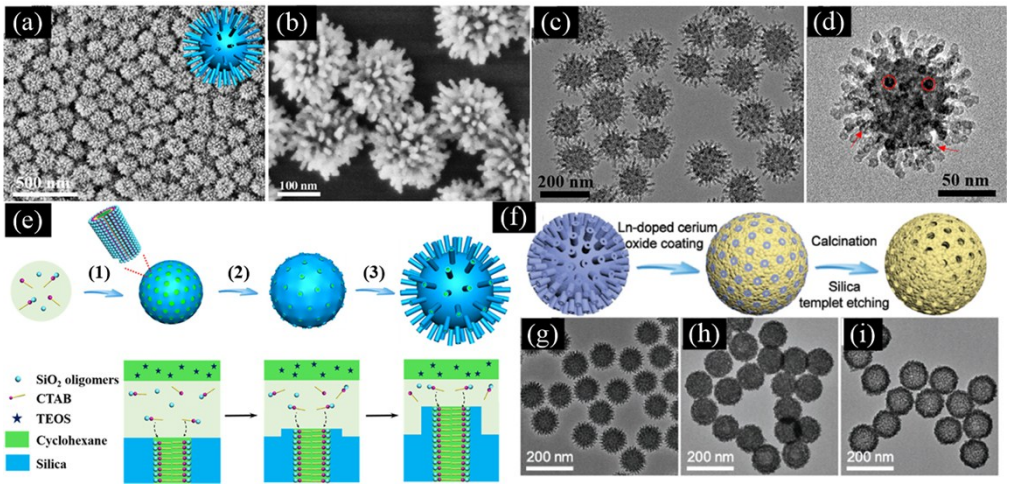

Fig. S3 SEM (a, b) and TEM (c, d) images of the virus-like mesoporous silica nanoparticles with different magnifications. The inset in (a) is the corresponding structural model. Schematic illustration of the formation process (e): (1) formation and growth of mesoporous silica nanoparticles, (2) formation of the nucleation sites, and (3) orientated growth of the silica nanotubes. (Reproduced from ref. 4 with permission from American Chemical Society, copyright 2017.). Schematic illustration of the synthesis procedure for lanthanide-doped hollow mesoporous cerium oxide nanoparticles (f). TEM images of original virus-like silica templates (g), virus-like silica with lanthanide-doped cerium hydroxide coating (h), lanthanide-doped hollow mesoporous cerium oxide nanoparticles after calcination and removing silica template (i). (Reproduced from ref. 5 with permission from John Wiley and Sons, copyright 2018.).

The inverse structures similar to models in Fig. 16a_3,b_3 or the so-defined virus-like or urchin-like could be discovered in silica mesoporous material. Zhang *et al*. successfully synthesized virus-like mesoporous silica NPs *via* a single-micelle epitaxial growth approach in an oil-water biphase system with low-concentration surfactants.[4] Fig. S3 showed SEM (a-b) and TEM (c-d) images of the as-fabricated uniform monodispersed virus-like mesoporous silica NPs, as well as the formation mechanism (e). Clearly, each unique virus-like morphology with particle size of about 160 nm included two geometrical structure parts, namely, an interior spherical core with *ca*. 110 nm diameter and separated peripheral nanotubes perpendicular to the core surface with about 35 nm length. The formation process of the as-prepared NPs underwent an isotropic growth under an ultralow surfactant concentration and an orientated growth (Fig. S3e), mainly embodying that (1) the formation of mesoporous

spherical silica; (2) the formation of nucleation sites on silica surfaces and the channels' necks; (3) single-micelle epitaxial growth of silica nanotubes on the nucleation sites. The virus-like products with unique internalization pathways owned more superior cellular uptake property and more enhanced blood circulation duration than that of conventional mesoporous silica. Furthermore, various core-shelled structured virus-like NPs could be realized on the basis of the epitaxial growth strategy, like Fe_3O_4@SiO_2, GO@SiO_2, Ag@SiO_2, Au@SiO_2, *etc*.[4] It was worthy to mention that these nanotubes on the surfaces of virus-like mesoporous silica were hollow and relatively uniform.[4] Very recently, a stepwise investigation was made by Zhang's team as well on the basis of the above results. In detail, virus-like silica nanospheres served as hard templates. Cerium hydroxide precursor doped with Yb^{3+} and Tm^{3+} was coated on their surfaces through a precipitation process. After calcination and silica etching, lanthanide-doped hollow mesoporous cerium oxide NPs were successfully developed as exhibited in Fig. S3f.[5] TEM images in Fig. S3g-i showed the structures of virus-like silica nanspheres, virus-like silica coated with lanthanide-doped cerium hydroxide, and lanthanide-doped hollow mesoporous cerium oxide nanospheres. The process could be simply considered as an opposite route from Fig. 16a_3 to a_1 except for template difference. The most important thing is that dendritic morphologies would appear in the as-fabricated hollow mesoporous cerium oxide nanospheres. These lanthanide-doped hollow mesoporous cerium oxide nanocatalysts could efficiently decompose the tumor's endogenous H_2O_2 to enhance photodynamic therapy in weak acidic tumour microenvironment. Dopants of Yb^{3+} and Tm^{3+} could trigger photocatalysis reactions with the assistance of cerium oxide matrix, giving rise to oxygen free radicals ($O_2^{\cdot-}$) and hydroxyl free radicals (·OH) that both induced cancer apoptosis. In addition, peptide modification from Arg-Gly-Asp accompanied with the unique architecture could also realize pH-responsive doxorubicin release in acid tumour sites and organelles of $\alpha_v\beta_3$ integrin-rich cancer cells for chemotherapy.[5]

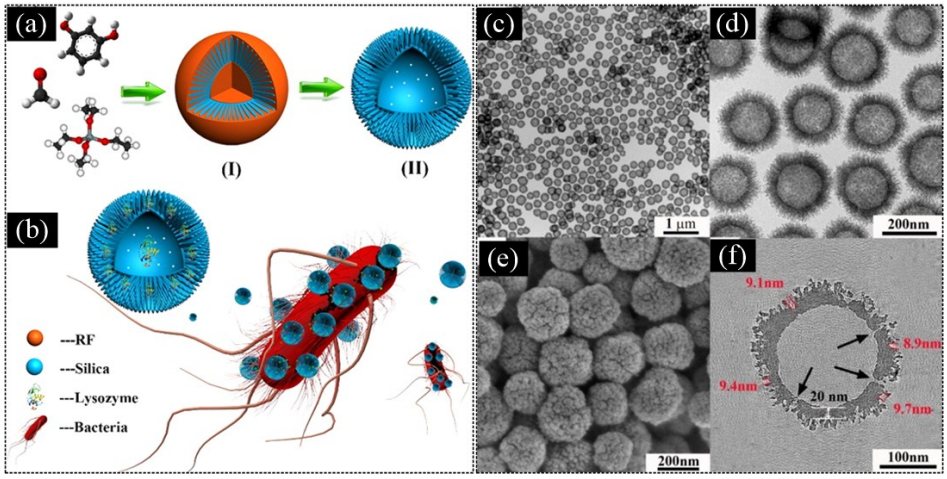

Fig. S4 (a) Schematic illustration of the synthesis of silica nanopollens, (b) efficient lysozyme delivery via silica nanopollens which are adhesive toward bacterial surfaces (size not to scale), (c,d) TEM images, (e) SEM image, and (f) ET slice of rough mesoporous silica hollow spheres (R-MSHSs). Reproduced from ref. 6 with permission from American Chemical Society, copyright 2016.

Yu *et al.* also fabricated a kind of mesoporous silica nanospheres with rough surfaces and named them as "silica nanopollens", because the morphology of the as-prepared NPs was extremely similar to that of the pollen.[6] Actually, it is hard to distinguish the as-obtained nanopollens from HDFNS spheres in TEM images either, but these nanopollens could be deemed as the inverse structures of HDFNS. Each nanopollen possessed a hollow inner cavity with a diameter of *ca*. 165 nm and a shell with the thickness of *ca*. 20 nm. In addition, some nanospikes located atop the nanopollen's outer surface (average diameter of 5 nm). A relatively denser silica shell could be achieved by easily tuning the amount of precursor TEOS. Due to the specific architecture of accessible hollow cavities and nanoscale surface roughness, the as-prepared nanopollens displayed enhanced adhesion toward bacteria and sustained lysozyme release, giving rise to a potent antibacterial activity and a prolonged bacterial inhibition up to 3 days toward *Escherichia coli*. Moreover, lysozyme-loaded silica nanopollens could achieve an excellent antimicrobial activity both *in vitro* and *ex vivo*.[6]

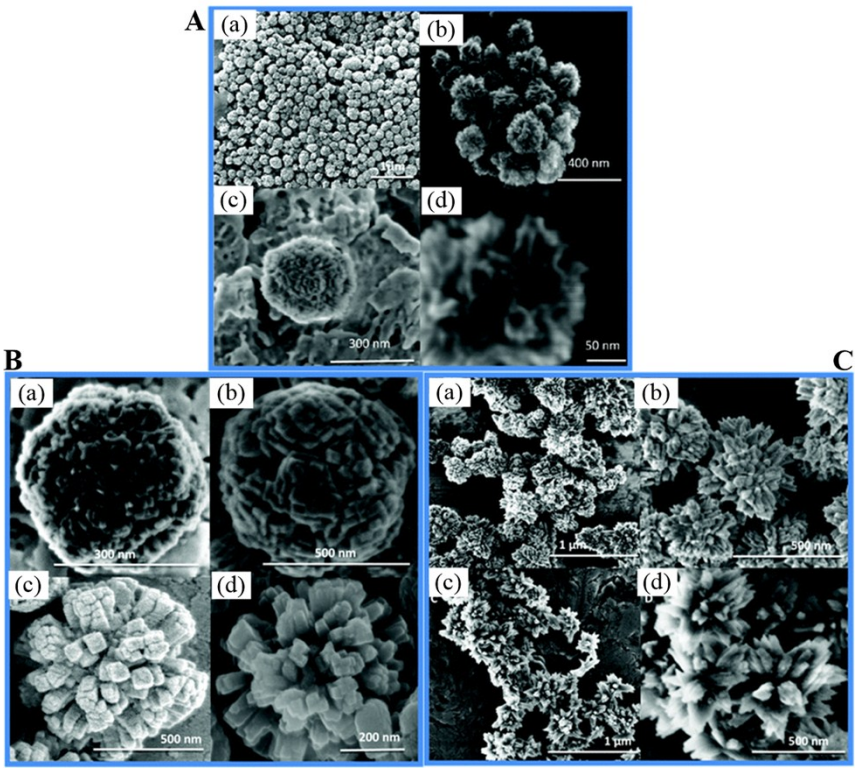

Fig. S5 (A) SEM images with different magnification of the anatase TiO_2 nanostructures obtained after microwave irradiation at 120 °C for 5 min. (B) SEM images of hierarchical TiO_2 nanostructures obtained after microwave irradiation at 120 °C for 30 min (a), 1 h (b), 2 h (c), and 3 h (d). (C) SEM images with different magnification of TiO_2 nanostructures obtained after microwave irradiation for 3 h at 100 °C (a,b) and 80 °C (c,d). Reproduced from ref. 7 with permission from The Royal Society of Chemistry, copyright 2012.

Analysis for “an evaporation-driven oriented assembly approach”.

In a typical synthesis,[8] Pluronic F127 ($PEO_{106}PPO_{70}PEO_{106}$), H_2O, acetic acid (HOAc), and concentrated HCl (36 wt%) were first dissolved in THF. Then, TBOT was added dropwise under vigorous stirring. Sequentially, the as-obtained solution was transferred into a volumetric flask and dried in an oven to evaporate THF stepwise. Nanospheres were prepared by further calcination. Pluronic F127 acted as templates, and this process could be termed as soft-templating method. SEM images in the original paper showed that the as-synthesized nanospheres were uniform with diameters of *ca*. 800 nm. The cylindrical open pores of *ca*. 5.5 nm were exposed on the outer surface of a certain nanosphere (the inset). The nanochannels were closely packed and arranged radially from the internal center to the outer surface, while another kind of pore embedded in the channels was observed and estimated to be 5-15 nm, discerned from high-angle annular dark-field scanning TEM (HAADFSTEM). The ultra-microtomed section of a single TiO_2 nanosphere was examined by using TEM technique. The resultant images in the original paper implied that the cylindrical pores were highly open and radially distributed along the restricted tangential direction, consistent with the SEM results. The growth of these unprecedented TiO_2 nanospheres with dendritic fibrous topographies was found to transform from spherically to radially cylindrical micelles by adjusting the solvent evaporation and confining the triblock copolymer hydrophilic boundary.

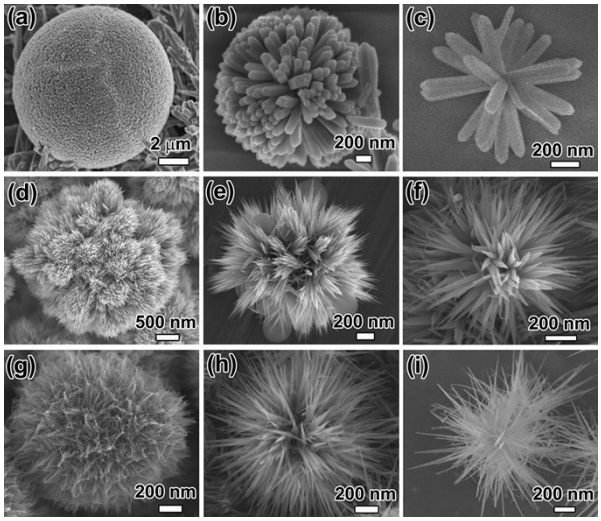

Fig. S6 SEM images of 3D dendritic nanostructures from TiO_2 mircospheres. (a-c) Microspheres had nanorod building units from reaction solutions with TTIP content increased. (d-f) Microspheres owned nanoribbon building units with EG increased and TTIP amount constant. (g-i) Microspheres possessed nanowire building units with TTIP and urea constant, but with EG increased. Reproduced from ref. 9 with permission from American Chemical Society, copyright 2011.

Kim *et al.* synthesized 3D spherical TiO_2 nanostructures with nanobranches surrounded through a simple hydrothermal synthesis by adjusting the precursor hydrolysis rate and the surfactant aggregation.[9] The as-prepared favorable architectures were also denoted as "dendritic" (Fig. S6), but with larger particle sizes above 2.0 μm. It could be clearly observed that nanorods (Fig. S6a-c), nanoribbons (Fig. S6d-f), and nanowires (Fig. S6g-i) as building units centrally radiated from their cores. Strictly speaking, various rod-like (Fig. S6a-c), cluster-like (Fig. S6d), and spear-like nanofibers (Fig. S6e-i) radially grew from their centers to the outer surfaces. The callings "fibrous" would be more appropriate as illustrated in 2.2.3.1.[10] These morphologies were directly observed from SEM images, while the TEM images were not provided therein. These textures could be controlled by tuning the compositions of the reaction solutions. Specifically, the varied pH value could control the aggregation of surfactants and the hydrolysis rate of the TiO_2 precursors. In detail, titanium

isopropoxide (TTIP), hydrochloric acid, CTAB, and water were used to fabricate NPs with dendritic nanorods. With a decreasing molar ratio of TTIP, the microspheres' diameter obviously decreased from 10 to 2.5 μm, and further to 1.8 μm. The microspheres seemed to be cracked by the nanorods. Ethylene glycol (EG) was added into the above solution to develop NPs with dendritic ribbons by controlling the aggregation structures of the surfactants and hydrolysis rate of precursors. With EG content increased, nanoribbon branches became sharp and well-defined. Urea as a slow-release basic reagent accompanied with EG was added for NPs with dendritic nanowires by adjusting the pH values of the reaction solutions. It was worth noting that urea ratios were identical for Fig. S6g-i, but with EG content increased. A higher EG amount simultaneously gave to smaller diameters and longer nanowires. Raman spectroscopy and XRD demonstrated that all TiO_2 nanostructures from the microspheres were well-crystallized in the rutile phase. HRTEM revealed that the exposed surfaces of the nanorods, nanoribbons and nanowires were (110) facets. These results indicated that EG and urea did affect crystal growth instead of the growth direction. EG played major roles in assisting crystal growth as a cosurfactant and retarding TTIP hydrolysis rate. Urea could reduce TTIP hydrolysis rate by increasing the solution pH by releasing OH^-. It was speculated that hydrolysis rate of TTIP in the reaction solutions follows the order of $TTIP_{aq}$> $TTIP_{aq}$+EG > $TTIP_{aq}$+EG+urea, resulting in NPs with different architectures.[9]

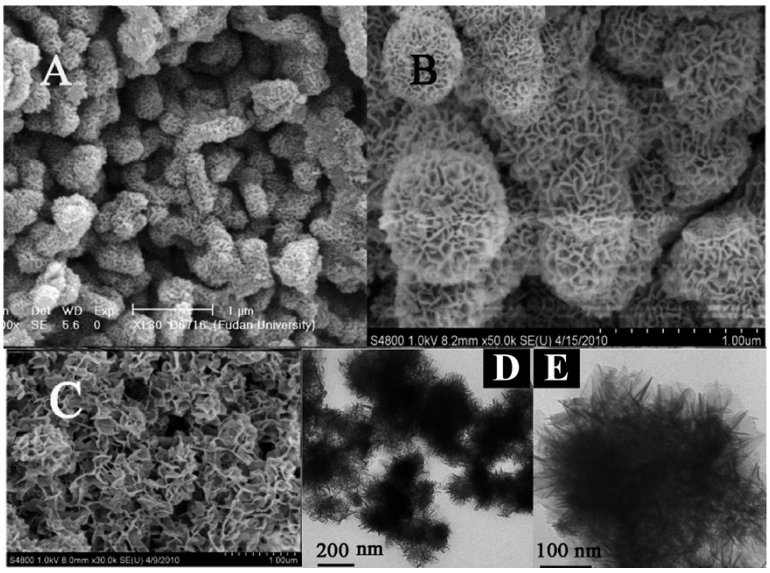

Fig. S7 SEM images of the hierarchical TiO_2 nanaparticles synthesized at 120 °C for (A) 1 h, (B) 6 h, and (C) 12 h, respectively. TEM images of calcined sample B at 200 nm (D) and 100 nm (E) scales, respectively. Reproduced from ref. 11 with permission from American Chemical Society, copyright 2011.

Wu *et al.* constructed flower-like hierarchical TiO_2 composed of abundant highly crystallized anatase nanocrystals *via* a one-step template-free hydrothermal method by replacing conventional Ti-containing precursors (such as titanium tetrachloride, titanium fluoride, titanium isopropoxide, and TBOT) with titanocene dichloride ($Ti(Cp)_2Cl_2$).[11] This substance was widely applied as metalorganic complex, but rarely as precursor to generate TiO_2. The existence of the two cyclopentadiene rings decreased its hydrolysis rate to a great degree, and thus became a beneficial factor to control the morphology. SEM images in Fig. S7 showed the morphological evolution of the as-prepared TiO_2 NPs. The intermediate products were quasi sphere-shaped with the sizes of about 350 nm and slightly aggregated at the first 1 h reaction time (Fig. S7A). As the reaction was prolonged to 6 h, spherical intermediates grow bigger with *ca.* 650 nm sizes in diameters (Fig. S7B). Particularly, a deal of thin nanosheets constituted their hierarchical structures in an interwoven style and exhibited relatively loose stacking compared to those yielded in the first stage. The morphology of these intermediate products awfully resembled DFNPs state with wrinkles in SEM, while totally differentiated in their TEM images (Fig. S7D,E). The products obtained from

12 h reaction almost collapsed and were even looser, indicating that this topography was not dendritic fibrous. As a result, it was speculated that $Ti(Cp)_2Cl_2$ first hydrolyzed and developed amorphous TiO_2 nanosheets, which quickly self-assembled into hierarchical flower-like nanostructures under Van der Waals interactions. Further grow-up made the nanosheets separated from one another because torsional stresses exceeded Van der Waals interactions (Fig. S7C).[11]

Reference:

1 X. Ding, Y. Wang and Y. Huang, *J. Harbin. Inst. Technol.*, 2018, **50**, 116-121 (Engineering Index, in chinese).

2 J. Yang, D. Shen, L. Zhou, W. Li, X. Li, C. Yao, R. Wang, A.M. Eltoni, F. Zhang and D. Zhao, *Chem. Mater.*, 2013, **25**, 3030-3037.

3 Q. Yue, J. Li, Y. Zhang, X. Cheng, X. Chen, P. Pan, J. Su, A.A. Elzatahry, A. Alghamdi, Y. Deng and D. Zhao, *J. Am. Chem. Soc.*, 2017,**139**, 15486-15493.

4 W. Wang, P. Wang, X. Tang, A.A. Elzatahry, S. Wang, D. Al-Dahyan, M. Zhao, C. Yao, C.-T. Hung, X. Zhu, T. Zhao, X. Li, F. Zhang and D. Zhao, *ACS Central Sci.*, 2017, **3**, 839-846.

5 C. Yao, W. Wang, P. Wang, M. Zhao, X. Li and F. Zhang, Adv. Mater., 2018, **30**, 1704833.

6 H. Song, Y.A. Nor, M. Yu, Y. Yang, J. Zhang, H. Zhang, C. Xu, N. Mitter and C. Yu, *J. Am. Chem. Soc.*, 2016, **138**, 6455-6462.

7 R. Rahal, A. Wankhade, D. Cha, A. Fihri, S. Ouldchikh, U. Patil and V. Polshettiwar, *RSC Adv.*, 2012, **2**, 7048-7052.

8 L. Yong, R. Che, C. Gang, J. Fan, Z. Sun, Z. Wu, M. Wang, B. Li, W. Jing and W. Yong, *Sci. Adv.*, 2015, **1**, 1500166.

9 Z. Sun, J.H. Kim, Y. Zhao, F. Bijarbooneh, V. Malgras, Y. Lee, Y.M. Kang and S.X. Dou, *J. Am. Chem. Soc.*, 2011, **133**, 19314-19317.

10 L.P. Xu, X. Wu, J. Meng, J. Peng, Y. Wen, X. Zhang and S. Wang, *Chem. Commun.*, 2013, **49**, 8752-8754.

11 T. Zhu, J. Li and Q. Wu, *ACS Appl. Mater. Inter.*, 2011, 3, 3448-3453.